Laser spectroscopy of triply charged ^{229}Th isomer for a nuclear clock

https://doi.org/10.1038/s41586-024-07296-1

Received: 24 September 2023

Accepted: 11 March 2024

Published online: 17 April 2024

Check for updates

Atsushi Yamaguchi[1,2,3]✉, Yudai Shigekawa[4], Hiromitsu Haba[4], Hidetoshi Kikunaga[5], Kenji Shirasaki[6], Michiharu Wada[7] & Hidetoshi Katori[1,2,8]

Thorium-229 (^{229}Th) possesses an optical nuclear transition between the ground state (^{229g}Th) and low-lying isomer (^{229m}Th). A nuclear clock based on this nuclear-transition frequency is expected to surpass existing atomic clocks owing to its insusceptibility to surrounding fields[1–5]. In contrast to other charge states, triply charged ^{229}Th (^{229}Th^{3+}) is the most suitable for highly accurate nuclear clocks because it has closed electronic transitions that enable laser cooling, laser-induced fluorescence detection and state preparation of ions[1,6–8]. Although laser spectroscopic studies of ^{229}Th^{3+} in the nuclear ground state have been performed[8], properties of ^{229m}Th^{3+}, including its nuclear decay lifetime that is essential to specify the intrinsic linewidth of the nuclear-clock transition, remain unknown. Here we report the trapping of ^{229m}Th^{3+} continuously supplied by a ^{233}U source and the determination of nuclear decay half-life of the isolated ^{229m}Th^{3+} to be $1{,}400^{+600}_{-300}$ s through nuclear-state-selective laser spectroscopy. Furthermore, by determining the hyperfine constants of ^{229m}Th^{3+}, we reduced the uncertainty of the sensitivity of the ^{229}Th nuclear clock to variations in the fine-structure constant by a factor of four. These results offer key parameters for the ^{229}Th^{3+} nuclear clock and its applications in the search for new physics.

The resonance frequency of nuclear transitions is highly insensitive to external electromagnetic fields owing to the smallness of the nuclear moments; thus, it is suitable for an atomic clock. Such a nuclear clock is expected to achieve unprecedented accuracy, exceeding current atomic clocks based on electronic transitions of atoms[1,5]. The low-energy nuclear transition between the ground state (^{229g}Th) and isomer (^{229m}Th) of ^{229}Th is regarded as a clock transition[1–4]. At present, the energy of ^{229m}Th has been determined to be approximately 8.3 eV by spectroscopy of internal conversion electrons[9], γ-ray spectroscopy[10–12] and vacuum ultraviolet (VUV) spectroscopy[13] of ^{229m}Th. Thus, this low-lying nuclear state can be excited using a VUV laser, allowing for high-precision laser spectroscopy. The ^{229}Th nuclear clock also has proposed uses as a highly sensitive sensor to search for dark matter[14,15], the fifth fundamental force[16] and variations in the fine-structure constant[17–19].

A laser-cooled ion in a trap is a suitable platform for a highly accurate clock because the strong confinement in a trap eliminates the Doppler effect and recoil effect[20]. Also, the internal state of the trapped ion can be initialized for clock operation by optical pumping. The necessary requirement here is the availability of closed electronic transitions. In contrast to ions in other charge states, triply charged ^{229}Th (^{229}Th^{3+}) possesses suitable closed electronic transitions for these operations[1,6,7]. However, crucial parameters for nuclear clocks, such as nuclear decay lifetime of ^{229m}Th^{3+}, remain unknown. This is partly because of the difficulties in preparing ^{229m}Th^{3+} by nuclear laser excitation and its optical detection. In this study, we overcome these difficulties by using ^{233}U as a source of ^{229m}Th^{3+} and developing a nuclear-state-selective laser spectroscopy technique that allows us to determine its nuclear decay lifetime and hyperfine constants.

Trapping of ^{229}Th^{3+} ions

Figure 1a shows our apparatus for trapping ^{229g}Th^{3+} and ^{229m}Th^{3+} ions, comprising ion preparation, transport and trap sections. The ^{229}Th^{3+} ions were obtained from a ^{233}U source[21–23] with a branching ratio ^{229g}Th:^{229m}Th ≈ 98%:2% (refs. 24,25). The ions were then cooled using helium buffer gas (2 kPa) and extracted as a low-energy ion beam using a radio-frequency (RF) carpet[26]. The extracted ions were transported using a quadrupole ion guide (QPIG) and captured using a linear Paul trap. For efficient ion trapping, the trap chamber was filled with helium buffer gas (0.2 Pa) and all measurements were conducted using helium buffer gas.

The ^{229}Th^{3+} ions were supplied to the trap at all times and the ions were confined by the entrance and exit endcaps by applying a voltage of 1.5 V. In this 'source on' operating mode, the fluorescence signal strength became constant over time because of the balance of loss and supply of the ^{229}Th^{3+} ions (Fig. 1b), allowing stable spectroscopic studies of the trapped ions. For the nuclear decay lifetime measurement of ^{229m}Th^{3+}, we stopped supplying ^{229}Th^{3+} by turning off the RF voltages applied to the RF carpet and QPIG. In this 'source off' mode, the fluorescence signal from the trapped ^{229}Th^{3+} ions decayed with a

[1]Quantum Metrology Laboratory, RIKEN, Wako, Japan. [2]RIKEN Center for Advanced Photonics, Wako, Japan. [3]PRESTO, Japan Science and Technology Agency, Kawaguchi, Japan. [4]Nishina Center for Accelerator-Based Science, RIKEN, Wako, Japan. [5]Research Center for Electron Photon Science, Tohoku University, Sendai, Japan. [6]Institute for Materials Research, Tohoku University, Sendai, Japan. [7]KEK Wako Nuclear Science Center, Wako, Japan. [8]Department of Applied Physics, Graduate School of Engineering, The University of Tokyo, Tokyo, Japan. ✉e-mail: atsushi.yamaguchi.fv@riken.jp

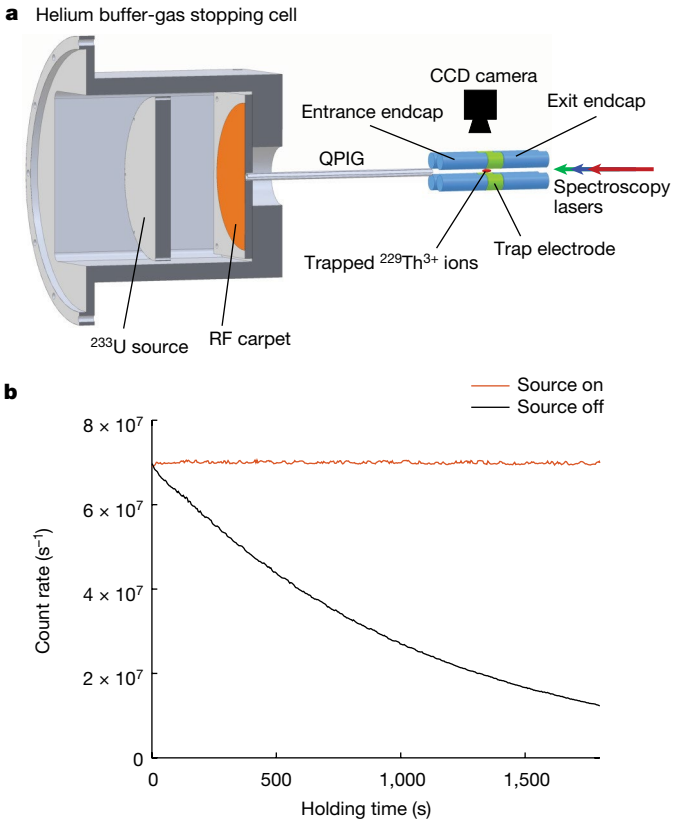

Fig. 1 | Trapping of continuously supplied $^{229}Th^{3+}$ ions. a, Schematic of the $^{229}Th^{3+}$ ion-trap system. The $^{229}Th^{3+}$ ions obtained as recoil ions from the ^{233}U source were collisionally cooled with a helium buffer gas (2 kPa). They were extracted by an RF carpet and transported to the linear Paul trap by a QPIG. Laser spectroscopy of trapped ions was performed by three lasers (wavelengths 1,088 nm, 690 nm and 984 nm), as indicated by three arrows. Fluorescence from ions at 984 nm was captured by a CCD camera. **b**, Fluorescence signal from the trapped $^{229}Th^{3+}$ ions as a function of holding time in two operating modes. In the 'source on' mode, ions were continuously supplied to the trap, leading to a stationary fluorescence signal. In the 'source off' mode, the supply of ions was stopped at time zero. In both operating modes, the entrance and exit endcaps (shown as light-blue electrodes in **a**) voltages were maintained at 1.5 V.

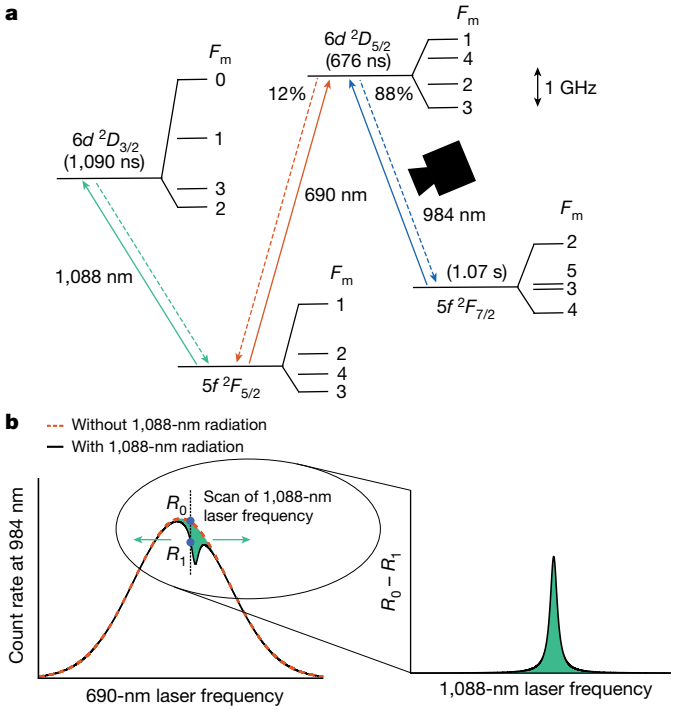

Fig. 2 | Laser spectroscopy of $^{229}Th^{3+}$. a, Electronic levels and transitions of $^{229}Th^{3+}$. The lifetimes of the excited states are calculated in ref. 45. The branching ratios from the $6d\,^2D_{5/2}$ state to the $5f^2F_{5/2}$ and $5f^2F_{7/2}$ states are calculated to be 12% and 88%, respectively. Owing to the nuclear spin $I_m = 3/2$, the fine-structure level of $^{229m}Th^{3+}$ is split into hyperfine states F_m. The hyperfine splitting was calculated on the basis of the hyperfine constants obtained in this study and shown with the indicator of 1 GHz. Solid and dashed lines between energy levels represent laser excitation and spontaneous emission. A CCD camera detected laser-induced fluorescence photons at 984 nm. **b**, Schematic describing the spectral-hole burning. By scanning the 1,088-nm laser frequency to move the position of the hole (horizontal green arrows) at which the 690-nm laser frequency was fixed (vertical dashed line) and recording fluorescence count rate at 984 nm with (R_1) and without (R_0) the 1,088-nm radiation, the high-resolution spectrum of the 1,088-nm hyperfine transition was obtained as $R_0 - R_1$.

lifetime ($1/e$) of approximately 15 min (Fig. 1b), which was attributed to reactions of Th^{3+} ions with impurity gasses[27].

Laser spectroscopy of $^{229}Th^{3+}$

Laser spectroscopy of $^{229}Th^{3+}$ was performed using the following three electronic transitions (Fig. 2a): $5f^2F_{5/2} \leftrightarrow 6d^2D_{3/2}$ (1,088 nm), $5f^2F_{5/2} \leftrightarrow 6d^2D_{5/2}$ (690 nm) and $5f^2F_{7/2} \leftrightarrow 6d^2D_{5/2}$ (984 nm).

The sub-Doppler spectrum of the hyperfine transition at 1,088 nm was obtained using saturated absorption spectroscopy. We burned a hole in the velocity distribution of the ions in the $5f^2F_{5/2}$ hyperfine state by applying a 1,088-nm laser. This hole was shelved to the $5f^2F_{7/2}$ state through the $6d^2D_{5/2}$ state driven by the 690-nm laser, for which the 984-nm laser was applied to detect laser-induced fluorescence. The detection process using the 984-nm transition optically pumps the ions to the $5f^2F_{5/2}$ state, because the branching ratios from the $6d^2D_{5/2}$ state to the $5f^2F_{5/2}$ and $5f^2F_{7/2}$ states are 12% and 88%, respectively (Fig. 2a). We note that using the 984-nm transition for fluorescence detection was crucial in nuclear-state-selective (^{229g}Th or ^{229m}Th) detection, as shown later.

We measured the spectrum of the 1,088-nm transition as shown in Fig. 2b. We fixed the 690-nm laser frequency (vertical dashed line) and scanned the 1,088-nm laser frequency, which moved the hole (shown as horizontal green arrows). If the position of the hole overlapped with the observation frequency (vertical dashed line), it was detected as $R_0 - R_1$. Here R_1 and R_0 are the fluorescence count rates with and without 1,088-nm radiation, respectively.

The frequency step of the 1,088-nm laser was 10 MHz. At each step, we measured R_1 and R_0 for 2 s. Covering the entire scan range of a few GHz typically required approximately an hour. We illuminated the 1,088-nm, 690-nm and 984-nm lasers onto the ions from the axial direction of the trap (copropagating configuration), as illustrated in Fig. 1a.

Nuclear-state-selective spectroscopy

For spectroscopy of the hyperfine structures of $^{229m}Th^{3+}$, we developed a spectroscopic technique that enabled selective detection of the $^{229m}Th^{3+}$ signal from the spectrum containing both $^{229g}Th^{3+}$ and $^{229m}Th^{3+}$ signals. In each scan of the 1,088-nm laser frequency, we used two different 984-nm laser frequencies, ν_A^{984} and ν_B^{984}. Figure 3a separately shows Doppler-broadened spectra of the 984-nm transition of $^{229g}Th^{3+}$ and $^{229m}Th^{3+}$ obtained by driving the 690-nm and 984-nm transitions. The 690-nm laser frequency was tuned to excite ions in the corresponding nuclear state. Different fluorescence strengths from each nuclear state at ν_A^{984} and ν_B^{984} allowed selective detection of the $^{229m}Th^{3+}$ signal and determination of its hyperfine constants.

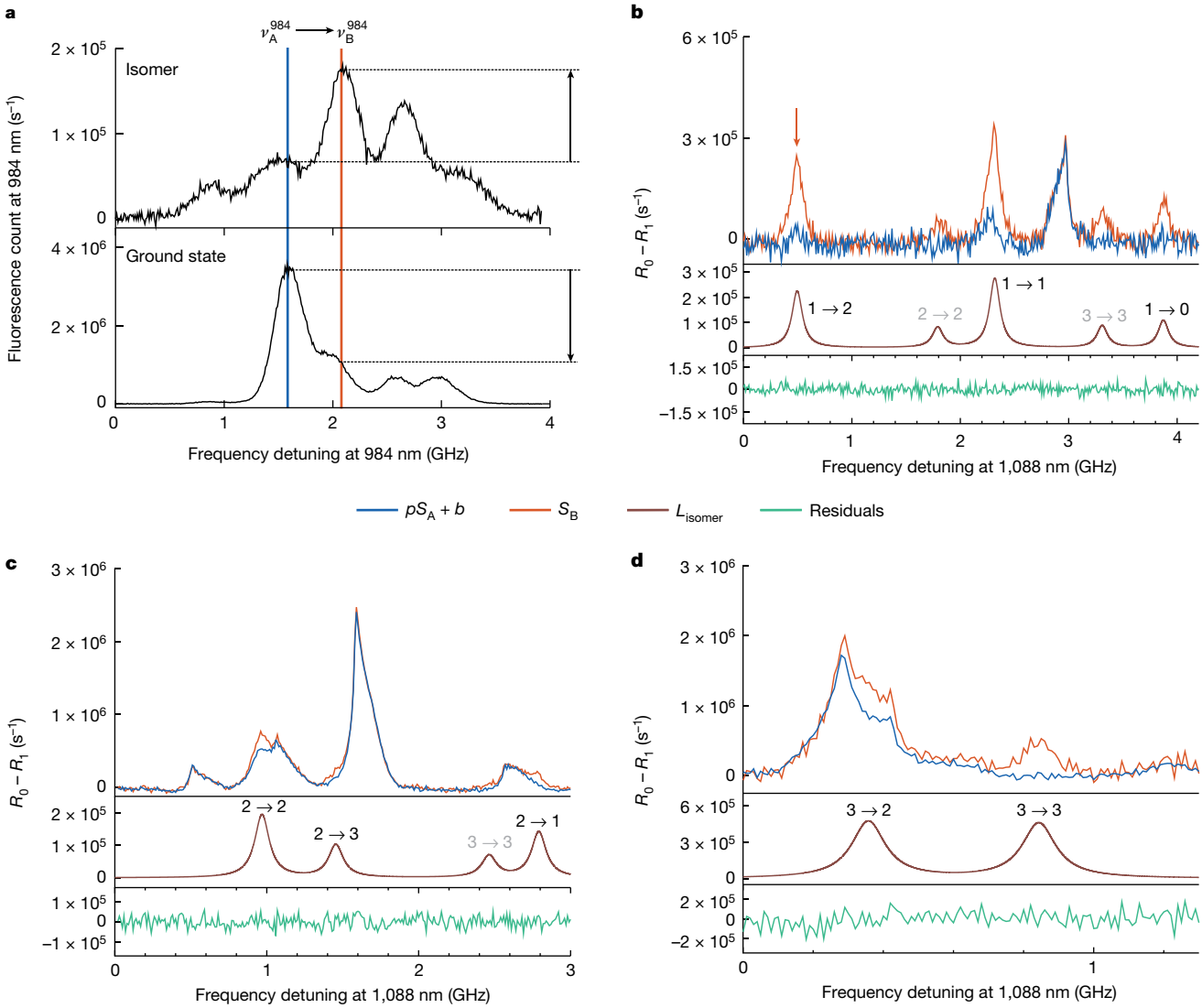

Fig. 3 | Observation of the hyperfine spectra of $^{229m}Th^{3+}$. **a**, Spectra of the 984-nm fluorescence transition are separately shown for $^{229}Th^{3+}$ in the nuclear ground state and isomer. The difference in fluorescence strength between the two nuclear states at ν_A^{984} and ν_B^{984} allowed detection of the isomer signal. **b**–**d**, We determined the hyperfine constants A_m and B_m of the $6d\,^2D_{3/2}$ state of $^{229m}Th^{3+}$ by fitting $pS_a + b + L_{isomer}$ to S_B. Here S_A and S_B are the hole-burning spectra of the 1,088-nm transition taken with ν_A^{984} and ν_B^{984}, respectively. The 690-nm laser was tuned to the (**b**) $|5f^2F_{5/2}, F_m = 1\rangle \rightarrow |6d\,^2D_{5/2}, F_m = 2\rangle$ (**b**), 2 → 3 (**c**) and 3 → 3 (**d**) transitions. L_{isomer} represents a group of Lorentzian curves describing the isomer peaks. The hyperfine constants were determined from the frequency intervals between the isomer peaks starting from the same hyperfine state (for example, 1 → 2, 1, 0 in **b**). Other isomer peaks (indicated with grey characters) starting from the different hyperfine states were not used to determine hyperfine constants and thus were treated as independent peaks. p is a scaling factor and b is an offset. The fitting result $pS_a + b$ (blue) is shown with S_B (orange). The brown and green curves represent the fitted L_{isomer} and residuals $S_B - (pS_a + b + L_{isomer})$, respectively. The hyperfine transitions $|5f\,^2F_{5/2}, F_m^i\rangle \rightarrow |6d\,^2D_{3/2}, F_m^f\rangle$ were labelled as $F_m^i \rightarrow F_m^f$. The orange arrow in **b** indicates the isomer peak used for the nuclear-decay-rate measurement.

Properties of $^{229m}Th^{3+}$

We determined hyperfine constants A_m (magnetic dipole) and B_m (electric quadrupole) of the $6d\,^2D_{3/2}$ state of $^{229m}Th^{3+}$ from three sets of hole-burning spectra S_A and S_B taken with ν_A^{984} and ν_B^{984}, as shown in Fig. 3b–d. We fitted $pS_A + b + L_{isomer}$ to S_B. Here $L_{isomer} = L_0(a_0, \nu_0, \gamma) + \sum_q L_q(a_q, \nu_0 + \Delta\nu_q(A_m, B_m), \gamma) + \sum_j L_j(a_j, \nu_j, \gamma)$ is a group of Lorentzian curves describing the isomer peaks. $a_{0,q,j}$, $\nu_{0,j}$ and γ denote the amplitude, centre frequency and width of the spectrum, respectively. We chose one of the isomer peaks in each of Fig. 3b–d as a reference peak L_0 (1 → 2 in Fig. 3b, 2 → 2 in Fig. 3c and 3 → 2 in Fig. 3d). $F_m^i \rightarrow F_m^f$ denotes the $|5f\,^2F_{5/2}, F_m^i\rangle \rightarrow |6d\,^2D_{3/2}, F_m^f\rangle$ transition. We used the frequency intervals $\Delta\nu_q(A_m, B_m)$ between L_0 and L_q starting from the same F_m^i (that is, L_q are 1 → 1, 0 in Fig. 3b, 2 → 3, 1 in Fig. 3c and 3 → 3 in Fig. 3d) to determine hyperfine constants. This is because these frequency intervals are determined only by the hyperfine constants of the $6d\,^2D_{3/2}$ state and are free from the hyperfine constants of the $5f^2F_{5/2}$ state. $\Delta\nu_q(A_m, B_m)$ was obtained from equation (1) in Methods. Other isomer peaks starting from different F_m^i (2 → 2 and 3 → 3 in Fig. 3b and 3 → 3 in Fig. 3c) did not contribute to the determination of the hyperfine constants and thus were treated as independent peaks L_j. Fitting parameters were the scaling factor p, offset b, $a_{0,q,j}$ and $\nu_{0,j}$ for each dataset and A_m, B_m and γ that were common in Fig. 3b–d. The results are

$$A_m(6d\,^2D_{3/2}) = -267(3)\ \text{MHz}$$
$$B_m(6d\,^2D_{3/2}) = 1,288(10)\ \text{MHz}$$

Next we determined the nuclear decay rate of $^{229m}Th^{3+}$ by taking the difference in the fluorescence decay rates between $^{229m}Th^{3+}$

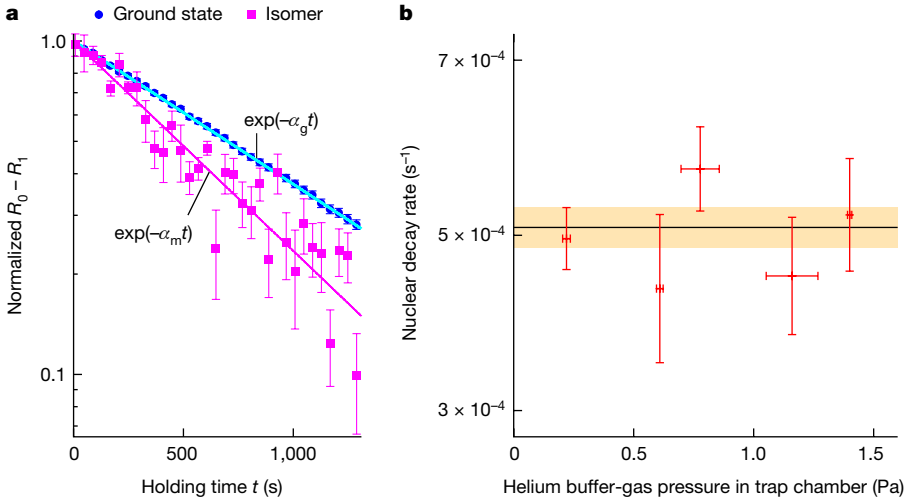

Fig. 4 | Determination of the nuclear decay rate of $^{229m}Th^{3+}$. The nuclear decay rate of $^{229m}Th^{3+}$ was determined by taking the difference in the decay rates between $^{229g}Th^{3+}$ (ground state) and $^{229m}Th^{3+}$ (isomer). **a**, Decay data are shown as functions of the ion holding time t. Both decay data were fitted by a single exponential function (exp(−αt)) to determine the decay rate α (cyan and pink curves for the ground-state and isomer data, respectively). The error bars represent the statistical uncertainties. **b**, Nuclear decay rates were investigated at various helium buffer-gas pressures in the trap chamber. The error bars represent the standard deviation of the mean. The horizontal black line and shaded area indicate the weighted average and error, respectively.

and $^{229g}Th^{3+}$. The 1/e decay rate α can be described by $\alpha_m = \alpha_c + \alpha_n$ for $^{229m}Th^{3+}$ and $\alpha_g = \alpha_c$ for $^{229g}Th^{3+}$. Here α_c is the decay rate of reactions between $^{229}Th^{3+}$ and impurity gasses[27]. Assuming that the decay rate α_c is same for α_m and α_g, the nuclear decay rate α_n can be derived by $\alpha_m - \alpha_g$.

To measure α_m, we used the spectrum corresponding to the $|5f^2F_{5/2}, F_m = 1\rangle \rightarrow |6d^2D_{3/2}, F_m = 2\rangle$ (1,088 nm) transition obtained with the $|5f^2F_{5/2}, F_m = 1\rangle \rightarrow |6d^2D_{5/2}, F_m = 2\rangle$ (690 nm) transition (the peak indicated by an orange arrow in Fig. 3b). This isomer peak is isolated 2.4 GHz away from the ground-state peak. As this is much larger than the spectral width, the overlap of the ground-state peak is negligible. The 984-nm laser frequency was fixed to ν_B^{984}. For α_g, the $|5f^2F_{5/2}, F_g = 5\rangle \rightarrow |6d^2D_{3/2}, F_g = 4\rangle$ (1,088 nm) transition taken with the $|5f^2F_{5/2}, F_g = 5\rangle \rightarrow |6d^2D_{5/2}, F_g = 5\rangle$ (690 nm) transition was used, in which the 984-nm laser frequency was fixed at ν_A^{984}. Because the nearest isomer peak is more than 550 MHz away, the contribution of the isomer peak is negligible. In both cases, we operated the trap in a 'source off' mode. Typical fluorescence decay signals are shown in Fig. 4a as a function of the holding time t. We note that the production of $^{229g}Th^{3+}$ by the nuclear decay of $^{229m}Th^{3+}$ in a trap had negligible effect on α_g owing to the small number of isomer ions. Also, no ions were extracted from the source to the trap in the 'source off' mode.

The loss of Th^{3+} by collision with argon and nitrogen depends on the electronic state of Th^{3+} (ref. 27). To evaluate the change of $\alpha_m - \alpha_g$ caused by this effect owing to different hyperfine structures between $^{229g}Th^{3+}$ and $^{229m}Th^{3+}$, we measured the dependence of α_m and α_g on the duration that ions spent in the excited electronic states (the $6d^2D_{3/2}$, $6d^2D_{5/2}$ and $5f^2F_{7/2}$ states) by changing the duty ratio of laser irradiation (Extended Data Fig. 2). Although no variations of α_m and α_g were observed within the measurement uncertainty, we evaluated the uncertainty of α_n resulting from this effect to be 1.5×10^{-4} s^{-1}.

We measured α_n in different helium gas pressures (in total, 11 decay measurements). Although we observed variations of α_g and α_m as we changed the helium gas pressure, the α_n was steady within the statistical errors, as shown in Fig. 4b. We thus attributed the variations of α_g and α_m to the variations of α_c caused by impurity gasses in the helium buffer gas. By taking a weighted average of the data in Fig. 4b, we determined the nuclear decay rate α_n to be $(5.1 \pm 1.5) \times 10^{-4}$ s^{-1}. This nuclear decay rate corresponds to the half-life (ln2/α_n) of $1{,}400^{+600}_{-300}$ s.

Discussion and outlook

By combining the hyperfine constants[8,28] of $^{229m}Th^{3+}$ with those of $^{229g}Th^{3+}$ and the nuclear moments of ^{229g}Th, the magnetic dipole moment and intrinsic electric quadrupole moment of ^{229m}Th was determined to be −0.378(8) μ_N and 8.84(10) eb. Here the nuclear parameters of ^{229g}Th (ref. 28) were obtained from hyperfine constants of $^{229g}Th^{3+}$ measured in ref. 8 and precision calculations. μ_N is the nuclear magneton and e is the elementary charge. The difference in the mean-square charge radii of the ^{229m}Th and ^{229g}Th ($\langle r^2_{229m}\rangle - \langle r^2_{229g}\rangle$) can be determined from the isomer shift $\Delta^{1,088}$ of the 1,088-nm transition. The isomer shift $\Delta^{1,088}$ is given by $\Delta^{1,088} = \nu_m^{1,088,C} - \nu_g^{1,088,C}$, in which $\nu_{m,g}^{1,088,C}$ is the centre frequency of the 1,088-nm transition in $^{229m,g}Th^{3+}$. Combined with $\nu_g^{1,088,C}$ reported in refs. 7,8, we determined $\Delta^{1,088}$ = 320(30) MHz, resulting in $\langle r^2_{229m}\rangle - \langle r^2_{229g}\rangle = 0.0097(26)$ fm^2. We used the conversion factor (field-shift constant) calculated in ref. 29. Details of the derivation of the nuclear properties are described in Methods. These nuclear parameters agree with those determined from the laser spectroscopy[25] of $^{229m}Th^{2+}$. To further confirm the validity of the results, we observed all remaining hyperfine resonance peaks of the 690-nm and 1,088-nm transitions at the frequencies calculated from our results (see Extended Data Fig. 4).

The nuclear decay half-life of $^{229m}Th^{3+}$ ($1{,}400^{+600}_{-300}$ s) corresponds to the natural linewidth $\Delta f = 80(20)$ μHz and the intrinsic quality (Q) factor $f_0/\Delta f = 2.5 \times 10^{19}$ of the nuclear transition with a transition frequency of $f_0 = 2.02$ PHz. This natural linewidth is more than an order of magnitude narrower than the linewidth of state-of-the-art ultrastable lasers[30].

The possible nuclear decay channels of $^{229m}Th^{3+}$ include internal conversion, alpha decay, electron bridge process and nuclear radiative decay (decay by VUV emission). For $^{229m}Th^{3+}$ in the electronic states used in this study, internal conversion decay was prohibited, because the ionization energy (approximately 29 eV) was higher than the isomer energy (8.3 eV). Theoretical predictions show that the alpha-decay rate[31] and electron-bridge rate[32,33] are small and that the dominant decay channel is nuclear radiative decay. Our result ($1{,}400^{+600}_{-300}$ s) was of the same order of magnitude as the previously predicted nuclear radiative decay rates[34–40]. The nuclear decay half-life of ^{229m}Th was reported to be 2,210(340) s based on the result of the VUV spectroscopy of ^{229m}Th in a MgF_2 crystal[13]. There, correction for refractive index

dependence was applied, although the applicability of the dependence is under investigation[13,41]. On the other hand, we obtained the nuclear decay half-life of $^{229m}Th^{3+}$ in the isolated environment, which differs from the previous studies using ^{229m}Th embedded on or in solid materials[13,42], for which nuclear decay half-life may be affected by the electronic structures of the solid materials.

The ^{229}Th nuclear clock is considered to possess an order-of-magnitude larger sensitivity (K) to variations in the fine-structure constant than that of existing atomic clocks ($K < 10$)[17,19], although the detailed mechanisms of this enhancement are still being investigated[43,44]. The sensitivity K can be derived from the change in the mean-square charge radii and electric quadrupole moment between ^{229g}Th and ^{229m}Th (ref. 29), yielding $K = 4(13) \times 10^3$, for which the uncertainty was improved by a factor of four compared with the previous study[25]. The dominant error is because of the uncertainties in the electric quadrupole moment of $^{229m}Th^{3+}$ and $^{229g}Th^{3+}$, which can be reduced by spectroscopy with laser-cooled $^{229m}Th^{3+}$ and $^{229g}Th^{3+}$ ions. Such investigations will establish a basis for searching for variations in the fine-structure constant.

Online content

Any methods, additional references, Nature Portfolio reporting summaries, source data, extended data, supplementary information, acknowledgements, peer review information; details of author contributions and competing interests; and statements of data and code availability are available at https://doi.org/10.1038/s41586-024-07296-1.

1. Peik, E. & Tamm, C. Nuclear laser spectroscopy of the 3.5 eV transition in Th-229. *Europhys. Lett.* **61**, 181–186 (2003).
2. Peik, E. & Okhapkin, M. Nuclear clocks based on resonant excitation of γ-transitions. *C. R. Phys.* **16**, 516–523 (2015).
3. Beeks, K. et al. The thorium-229 low-energy isomer and the nuclear clock. *Nat. Rev. Phys.* **3**, 238–248 (2021).
4. Peik, E. et al. Nuclear clocks for testing fundamental physics. *Quantum Sci. Technol.* **6**, 034002 (2021).
5. Campbell, C. J. et al. Single-ion nuclear clock for metrology at the 19th decimal place. *Phys. Rev. Lett.* **108**, 120802 (2012).
6. Klinkenberg, P. F. A. Spectral structure of trebly ionized thorium, Th IV. *Physica B+C* **151**, 552–567 (1988).
7. Campbell, C. J. et al. Multiply charged thorium crystals for nuclear laser spectroscopy. *Phys. Rev. Lett.* **102**, 233004 (2009).
8. Campbell, C. J., Radnaev, A. G. & Kuzmich, A. Wigner crystals of ^{229}Th for optical excitation of the nuclear isomer. *Phys. Rev. Lett.* **106**, 223001 (2011).
9. Seiferle, B. et al. Energy of the ^{229}Th nuclear clock transition. *Nature* **573**, 243–246 (2019).
10. Beck, B. R. et al. Energy splitting of the ground-state doublet in the nucleus ^{229}Th. *Phys. Rev. Lett.* **98**, 142501 (2007).
11. Yamaguchi, A. et al. Energy of the ^{229}Th nuclear clock isomer determined by absolute γ-ray energy difference. *Phys. Rev. Lett.* **123**, 222501 (2019).
12. Sikorsky, T. et al. Measurement of the ^{229}Th isomer energy with a magnetic microcalorimeter. *Phys. Rev. Lett.* **125**, 142503 (2020).
13. Kraemer, S. et al. Observation of the radiative decay of the ^{229}Th nuclear clock isomer. *Nature* **617**, 706–710 (2023).
14. Arvanitaki, A., Huang, J. & Van Tilburg, K. Searching for dilaton dark matter with atomic clocks. *Phys. Rev. D* **91**, 015015 (2015).
15. Tsai, Y.-D., Eby, J. & Safronova, M. S. Direct detection of ultralight dark matter bound to the Sun with space quantum sensors. *Nat. Astron.* **7**, 113–121 (2023).
16. Brzeminski, D., Chacko, Z., Dev, A., Flood, I. & Hook, A. Searching for a fifth force with atomic and nuclear clocks. *Phys. Rev. D* **106**, 095031 (2022).
17. Flambaum, V. V. Enhanced effect of temporal variation of the fine structure constant and the strong interaction in ^{229}Th. *Phys. Rev. Lett.* **97**, 092502 (2006).
18. Safronova, M. S. et al. Search for new physics with atoms and molecules. *Rev. Mod. Phys.* **90**, 025008 (2018).
19. Fadeev, P., Berengut, J. C. & Flambaum, V. V. Sensitivity of ^{229}Th nuclear clock transition to variation of the fine-structure constant. *Phys. Rev. A* **102**, 052833 (2020).
20. von der Wense, L. & Seiferle, B. The ^{229}Th isomer: prospects for a nuclear optical clock. *Eur. Phys. J. A* **56**, 277 (2020).
21. von der Wense, L., Seiferle, B., Laatiaoui, M. & Thirolf, P. G. Determination of the extraction efficiency for ^{233}U source α-recoil ions from the MLL buffer-gas stopping cell. *Eur. Phys. J. A* **51**, 29 (2015).
22. von der Wense, L. et al. Direct detection of the ^{229}Th nuclear clock transition. *Nature* **533**, 47–51 (2016).
23. von der Wense, L., Seiferle, B., Laatiaoui, M. & Thirolf, P. G. The extraction of $^{229}Th^{3+}$ from a buffer-gas stopping cell. *Nucl. Instrum. Methods Phys. Res. B* **376**, 260–264 (2016).
24. Barci, V. et al. Nuclear structure of ^{229}Th from γ-ray spectroscopy study of ^{233}U α-particle decay. *Phys. Rev. C* **68**, 034329 (2003).
25. Thielking, J. et al. Laser spectroscopic characterization of the nuclear-clock isomer ^{229m}Th. *Nature* **556**, 321–325 (2018).
26. Wada, M. et al. Slow RI-beams from projectile fragment separators. *Nucl. Instrum. Methods Phys. Res. B* **204**, 570–581 (2003).
27. Churchill, L. R., DePalatis, M. V. & Chapman, M. S. Charge exchange and chemical reactions with trapped Th^{3+}. *Phys. Rev. A* **83**, 012710 (2011).
28. Porsev, S. G., Safronova, M. S. & Kozlov, M. G. Precision calculation of hyperfine constants for extracting nuclear moments of ^{229}Th. *Phys. Rev. Lett.* **127**, 253001 (2021).
29. Berengut, J. C., Dzuba, V. A., Flambaum, V. V. & Porsev, S. G. Proposed experimental method to determine α sensitivity of splitting between ground and 7.6 eV isomeric states in ^{229}Th. *Phys. Rev. Lett.* **102**, 210801 (2009).
30. Zhang, W. et al. Ultrastable silicon cavity in a continuously operating closed-cycle cryostat at 4 K. *Phys. Rev. Lett.* **119**, 243601 (2017).
31. Dykhne, A. M., Eremin, N. V. & Tkalya, E. V. Alpha decay of the first excited state of the Th-229 nucleus. *J. Exp. Theor. Phys. Lett.* **64**, 345–349 (1996).
32. Porsev, S. G. & Flambaum, V. V. Effect of atomic electrons on the 7.6-eV nuclear transition in $^{229}Th^{3+}$. *Phys. Rev. A* **81**, 032504 (2010).
33. Müller, R. A., Volotka, A. V., Fritzsche, S. & Surzhykov, A. Theoretical analysis of the electron bridge process in $^{229}Th^{3+}$. *Nucl. Instrum. Methods Phys. Res. B* **408**, 84–88 (2017).
34. Dykhne, A. M. & Tkalya, E. V. Matrix element of the anomalously low-energy (3.5±0.5 eV) transition in ^{229}Th and the isomer lifetime. *J. Exp. Theor. Phys. Lett.* **67**, 251–256 (1998).
35. Ruchowska, E. et al. Nuclear structure of ^{229}Th. *Phys. Rev. C* **73**, 044326 (2006).
36. Tkalya, E. V., Schneider, C., Jeet, J. & Hudson, E. R. Radiative lifetime and energy of the low-energy isomeric level in ^{229}Th. *Phys. Rev. C* **92**, 054324 (2015).
37. Minkov, N. & Pálffy, A. Reduced transition probabilities for the gamma decay of the 7.8 eV isomer in ^{229}Th. *Phys. Rev. Lett.* **118**, 212501 (2017).
38. Minkov, N. & Pálffy, A. Theoretical predictions for the magnetic dipole moment of ^{229m}Th. *Phys. Rev. Lett.* **122**, 162502 (2019).
39. Minkov, N. & Pálffy, A. ^{229m}Th isomer from a nuclear model perspective. *Phys. Rev. C* **103**, 014313 (2021).
40. Shigekawa, Y. et al. Estimation of radiative half-life of ^{229m}Th by half-life measurement of other nuclear excited states in ^{229}Th. *Phys. Rev. C* **104**, 024306 (2021).
41. Tkalya, E. V. Spontaneous emission probability for $M1$ transition in a dielectric medium: $^{229m}Th(3/2^+, 3.5\pm1.0\ eV)$ decay. *J. Exp. Theor. Phys. Lett.* **71**, 311–313 (2000).
42. Seiferle, B., von der Wense, L. & Thirolf, P. G. Lifetime measurement of the ^{229}Th nuclear isomer. *Phys. Rev. Lett.* **118**, 042501 (2017).
43. Hayes, A. C., Friar, J. L. & Möller, P. Splitting sensitivity of the ground and 7.6 eV isomeric states of ^{229}Th. *Phys. Rev. C* **78**, 024311 (2008).
44. Litvinova, E., Feldmeier, H., Dobaczewski, J. & Flambaum, V. Nuclear structure of lowest ^{229}Th states and time-dependent fundamental constants. *Phys. Rev. C* **79**, 064303 (2009).
45. Safronova, U. I., Johnson, W. R. & Safronova, M. S. Excitation energies, polarizabilities, multipole transition rates, and lifetimes in Th IV. *Phys. Rev. A* **74**, 042511 (2006).

Publisher's note Springer Nature remains neutral with regard to jurisdictional claims in published maps and institutional affiliations.

Springer Nature or its licensor (e.g. a society or other partner) holds exclusive rights to this article under a publishing agreement with the author(s) or other rightsholder(s); author self-archiving of the accepted manuscript version of this article is solely governed by the terms of such publishing agreement and applicable law.

© The Author(s), under exclusive licence to Springer Nature Limited 2024

Methods

Extraction and trapping of $^{229}Th^{3+}$ ions

As the ion source for $^{229}Th^{3+}$, we used ^{233}U, which contained 0.226(2) ppm ^{232}U. The 600 kBq of ^{233}U was electrodeposited on a titanium foil (thickness 50 μm). Before the electrodeposition process, we chemically purified ^{233}U with an ion-exchange resin to remove the decay products of ^{233}U and ^{232}U. The diameter of the deposited area was 90 mm. The ^{233}U source was then heated at 600 °C for two days in a vacuum (10^{-4}–10^{-5} Pa) to remove impurities attached during the electrodeposition process. The ^{233}U source was prepared in March 2021. All measurements presented in this study were conducted between September 2022 and July 2023.

Recoil $^{229}Th^{3+}$ ions emitted from the surface of the ^{233}U source were cooled using helium buffer gas (2 kPa). Collisionally cooled $^{229}Th^{3+}$ ions were collected using an RF carpet[26] using a push field. The distance between the ^{233}U source and RF carpet was 5 cm and the gradient of the push field was 28 V cm^{-1}. The RF carpet was made of a printed circuit board (PCB) with a centre hole surrounded by concentric ring electrodes. The diameter of the centre hole is 240 μm. The width and interval of electrodes are 30 μm and 130 μm, respectively. We applied an RF voltage to each electrode (frequency 12.1 MHz, amplitude 45 V_{pp}). Voltages at the neighbouring electrodes were out of phase by 180°, producing an electromagnetic barrier on the surface of the RF carpet against $^{229}Th^{3+}$ ions. To extract ions efficiently, we used an 'ion-surfing' technique[46]. A potential wave travelling to the centre hole was generated by superimposing a phase-shifted low-frequency voltage (200 kHz) on every four ring electrodes with 90° phase shifts.

The extracted ions were then transported to traps using a QPIG. The QPIG module made of a PCB was segmented to create a voltage gradient (0.2 V cm^{-1}) to transport ions efficiently. The width and length of each QPIG module were 2 and 120 mm, respectively. The QPIG module was connected to a linear Paul trap operated with an RF voltage with frequency and amplitude of 2.4 MHz and 700 V_{pp}, respectively. The length and diameter of each of the four rods of the trap electrode were both 10 mm and the diameter of the trap area was 8.8 mm. The lengths of the entrance and exit endcap electrodes are 53 and 83 mm, respectively. The incoming rate of $^{229}Th^{3+}$ ions and trapping efficiency was estimated to be about 2,000 ions s^{-1} and 40%, respectively. The trap chamber was continuously supplied with helium buffer gas and simultaneously evacuated using a turbomolecular pump. Furthermore, to suppress reactions of Th^{3+} with impurity gasses, a getter pump (SAES Getters, Z1000) was installed in a trap chamber. We used 99.99995 vol% pure helium as a buffer gas, which was further purified by two gas purifier systems.

Laser spectroscopy

All three lasers used for spectroscopy (wavelengths: 1,088 nm, 690 nm and 984 nm) were semiconductor lasers pre-stabilized by grating feedback. All laser frequencies were stabilized to individual 10-cm reference cavities. The laser frequency was measured and controlled using a wavemeter (HighFinesse WSU-2). The feedback signal from the wavemeter was applied to a piezoelectric transducer to define the mirror spacing of the reference cavity. A Rb-stabilized distributed feedback laser calibrated the wavemeter every two minutes.

Typical laser intensities at the position of ions were estimated to be 3 W cm^{-2} for 1,088 nm, 0.6 W cm^{-2} for 690 nm and 0.3 W cm^{-2} for 984 nm. Laser-induced fluorescence photons at 984 nm from $^{229}Th^{3+}$ ions were captured by a charge-coupled device (CCD) camera through an optical bandpass filter with 80% transmission at 980 ± 10 nm. All other light in the range 200–1,200 nm were blocked. The quantum efficiency of the camera at 984 nm was approximately 20%.

Extended Data Fig. 1 shows the Doppler-broadened spectrum of the $5f^2F_{5/2} \leftrightarrow 6d^2D_{5/2}$ transition (690 nm) of $^{229g}Th^{3+}$. The 690-nm laser was scanned with a frequency step of 10 MHz, whereas the 984-nm laser frequency was fixed at ν_A^{984} (the 1,088-nm laser was turned off). The average time required for each frequency step was 2 s. The $5f^2F_{5/2} \leftrightarrow 6d^2D_{5/2}$ transition (690 nm) of $^{229g}Th^{3+}$ comprises the 15 hyperfine transitions indicated by vertical blue bars. We fit a single Gaussian function to the isolated peak (the peak labelled 5 → 4) and determined its full width at half maximum to be 410 MHz. Assuming that this width was primarily caused by the Doppler effect, the ion cloud temperature was estimated to be 400 K (corresponding to 0.034 eV). The black curve in Extended Data Fig. 1 represents S, defined by the following equation:

$$S = p_g[r_1G_1(x_1, \sigma) + r_2G_2(x_2, \sigma) + \cdots + r_{15}G_{15}(x_{15}, \sigma)],$$

in which p_g is a global scaling factor, x_i and r_i are the centre frequency and the calculated cross-section, respectively, of the ith hyperfine transition, G_i is a Gaussian function and σ is its standard deviation. We used p_g and σ determined by fitting of the isolated 5 → 4 spectrum. x_i was fixed to the values reported in refs. 7,8.

We also took the Doppler-broadened spectrum of the $5f^2F_{7/2} \leftrightarrow 6d^2D_{5/2}$ transition (984 nm) of $^{229g}Th^{3+}$ and $^{229m}Th^{3+}$ by scanning the 984-nm laser frequency with a 10-MHz step (Fig. 3a). For $^{229g}Th^{3+}$, the 690-nm laser frequency was fixed at the $|5f^2F_{5/2}, F_g = 5\rangle \rightarrow |6d^2D_{5/2}, F_g = 4\rangle$ transition. For the $^{229m}Th^{3+}$ spectrum, isomer ions were excited by the $|5f^2F_{5/2}, F_m = 1\rangle \rightarrow |6d^2D_{5/2}, F_m = 2\rangle$ transition. Here the 690-nm laser frequency was detuned by +240 MHz to avoid excitation of the $^{229g}Th^{3+}$ ions through the neighbouring $|5f^2F_{5/2}, F_g = 5\rangle \rightarrow |6d^2D_{5/2}, F_g = 4\rangle$ and $|5f^2F_{5/2}, F_g = 5\rangle \rightarrow |6d^2D_{5/2}, F_g = 5\rangle$ transitions, both of which were more than 750 MHz away from the laser frequency.

During spectroscopy, ions can be optically pumped to the dark hyperfine state, at which they do not absorb laser photons. Even in such a situation, we observed a fluorescence signal, which was attributed to hyperfine-changing collisions between $^{229}Th^{3+}$ and the helium buffer gas.

Determination of hyperfine constants

Hyperfine splitting can be expressed by a magnetic dipole constant A and an electric quadrupole constant B. The contribution of other higher-order multipolarities is negligible compared with the measurement uncertainty of this study. The $A_{g,m}$ and $B_{g,m}$ for $^{229g,m}Th^{3+}$ are given by[47]

$$A_{g,m} = \left(\frac{\mu_{g,m}}{I_{g,m}}\right)\frac{H(0)}{J} = \left(\frac{\mu_{g,m}}{I_{g,m}}\right)A^{ele}$$
$$B_{g,m} = Q^s_{g,m}\varphi(0) = Q^s_{g,m}B^{ele}.$$

Here $\mu_{g,m}$ and $Q^s_{g,m}$ are the magnetic dipole moment and spectroscopic electric quadrupole moment, respectively, of nuclei of the nuclear ground (g) and isomeric (m) state, J is the total electronic angular moment, $H(0)$ represents the magnetic field produced by electrons in the nucleus, $\varphi(0)$ is the gradient at the nucleus of the electric field of the orbital electrons. The electronic factors are separated into A^{ele} and B^{ele}. Because A^{ele} is common to A_g and A_m, the ratio $A_m/A_g = (\mu_m/\mu_g)(I_g/I_m)$ does not depend on the electronic state and charge state. The same is true for B_m/B_g. This feature was used to convert the hyperfine constants of the $6d^2D_{3/2}$ state into those of other electronic states.

The resonance frequency of the transition λ (λ = 1,088 nm, 690 nm and 984 nm) between the hyperfine levels F^i_s and F^f_s (s = m and g for $^{229m}Th^{3+}$ and $^{229g}Th^{3+}$, respectively) is described by

$$\nu^{\lambda}_{s,\mathrm{HF}}(I_s, J^{\mathrm{i}}_s, F^{\mathrm{i}}_s, J^{\mathrm{f}}_s, F^{\mathrm{f}}_s) = \nu^{\lambda,\mathrm{C}}_s + \left[A^{\mathrm{f}}_s\left(\frac{K^{\mathrm{f}}_s}{2}\right) + B^{\mathrm{f}}_s\left\{\frac{\left(\frac{3}{2}\right)K^{\mathrm{f}}_s(K^{\mathrm{f}}_s+1) - 2I_s(I_s+1)J^{\mathrm{f}}_s(J^{\mathrm{f}}_s+1)}{4I_s(2I_s-1)J^{\mathrm{f}}_s(2J^{\mathrm{f}}_s-1)}\right\}\right] - \left[A^{\mathrm{i}}_s\left(\frac{K^{\mathrm{i}}_s}{2}\right) + B^{\mathrm{i}}_s\left\{\frac{\left(\frac{3}{2}\right)K^{\mathrm{i}}_s(K^{\mathrm{i}}_s+1) - 2I_s(I_s+1)J^{\mathrm{i}}_s(J^{\mathrm{i}}_s+1)}{4I_s(2I_s-1)J^{\mathrm{i}}_s(2J^{\mathrm{i}}_s-1)}\right\}\right] \quad (1)$$

$$\nu^{\lambda,\mathrm{C}}_{\mathrm{m}} = \nu^{\lambda,\mathrm{C}}_{\mathrm{g}} + \Delta^{\lambda}.$$

Here $\nu^{\lambda,\mathrm{C}}_s$ is the centre frequency, Δ^{λ} is the isomer shift and $K^{\mathrm{i,f}}_s = F^{\mathrm{i,f}}_s(F^{\mathrm{i,f}}_s+1) - I_s(I_s+1) - J^{\mathrm{i,f}}_s(J^{\mathrm{i,f}}_s+1)$.

To determine hyperfine constants, we first needed to assign $F^{\mathrm{i}} \rightarrow F^{\mathrm{f}}$ to each isomer peak. This F-number assignment was carried out by fitting the resonance frequencies of all observed isomer peaks for all possible combinations of $F^{\mathrm{i}} \rightarrow F^{\mathrm{f}}$. We adopted the $F^{\mathrm{i}} \rightarrow F^{\mathrm{f}}$ combination that gave the smallest fitting residuals. The validity of this assignment was also checked by the selection rules in the 690-nm and 1,088-nm transitions. Once $F^{\mathrm{i}} \rightarrow F^{\mathrm{f}}$ was assigned, we determined A_{m} and B_{m} by fitting using the three datasets of S_{A} and S_{B} (Fig. 3b–d) as described in the main text. To preserve statistical information in S_{A} and S_{B}, we determined hyperfine constants by a single fitting including the scaling factor p.

We note that, in the obtained spectra in Fig. 3b–d, the frequency intervals between the hyperfine peaks were preserved even if the frequency of the 690-nm laser was not accurately set to the corresponding hyperfine resonance for the following reasons.

In this study, ions were irradiated with 1,088-nm and 690-nm lasers in a copropagating configuration. In this configuration, the relations between the resonance frequencies of the 1,088-nm ($\nu^{1,088}_{s,\mathrm{HF}}$) and 690-nm ($\nu^{690}_{s,\mathrm{HF}}$) transitions can be described by

$$\nu^{1,088}_{\mathrm{L}} = \nu^{1,088}_{s,\mathrm{HF}} + (k^{1,088}/k^{690})(\nu^{690}_{\mathrm{L}} - \nu^{690}_{s,\mathrm{HF}}) \quad (2)$$

in which $\nu^{1,088}_{\mathrm{L}}$ and ν^{690}_{L} are the 1,088-nm and 690-nm laser frequencies, respectively, and $k^{1,088}$ and k^{690} are their wavenumbers[25]. The detailed description of $\nu^{\lambda}_{s,\mathrm{HF}}$ is shown in equation (1).

We scanned $\nu^{1,088}_{\mathrm{L}}$ within only a few GHz with a fixed ν^{690}_{L}. In this case, the second term on the right side of equation (2) can be regarded as a constant term because the change of $(k^{1,088}/k^{690})(\nu^{690}_{\mathrm{L}} - \nu^{690}_{s,\mathrm{HF}})$ is on the order of 100 Hz, which is negligible compared with the measurement uncertainty. As a result, intervals of two resonances of the 1,088-nm spectrum, for example, $\nu^{1,088}_{\mathrm{m,HF}}(b) - \nu^{1,088}_{\mathrm{m,HF}}(a)$ for resonances a and b, can be obtained by $\nu^{1,088}_{\mathrm{L}}(b) - \nu^{1,088}_{\mathrm{L}}(a)$, which does not depend on ν^{690}_{L}. This is because $(k^{1,088}/k^{690})(\nu^{690}_{\mathrm{L}} - \nu^{690}_{s,\mathrm{HF}})$ is removed as a common term.

Isomer shift

The isomer shift of the $5f^2F_{5/2} \leftrightarrow 6d^2D_{3/2}$ transition (1,088 nm) is expressed as $\Delta^{1,088} = \nu^{1,088,\mathrm{C}}_{\mathrm{m}} - \nu^{1,088,\mathrm{C}}_{\mathrm{g}}$. Here the centre frequency $\nu^{1,088,\mathrm{C}}_{\mathrm{m}}$ can be obtained by setting $A_{\mathrm{m}} = B_{\mathrm{m}} = 0$ in $\nu^{1,088}_{\mathrm{m,HF}}$ (equation (1)). As can be seen in equation (2), to determine $\nu^{1,088}_{\mathrm{m,HF}}$, we need to set the 690-nm laser frequency (ν^{690}_{L}) to $\nu^{690}_{\mathrm{m,HF}}$. We thus first determined $\nu^{690}_{\mathrm{m,HF}}$ of the $|^2F_{5/2}, F_{\mathrm{m}} = 1\rangle \rightarrow |^2D_{5/2}, F_{\mathrm{m}} = 2\rangle$ transition by taking the spectra of the 1,088-nm transition with several different ν^{690}_{L} (Extended Data Fig. 3a). Then, $\nu^{690}_{\mathrm{m,HF}}$ was determined to be ν^{690}_{L}, which yielded the largest signal strength (spectral area) for the 1,088-nm spectra, as shown in Extended Data Fig. 3b. We set the ν^{690}_{L} to $\nu^{690}_{\mathrm{m,HF}}$ and measured the spectra of the 1,088-nm transition to obtain $\nu^{1,088}_{\mathrm{m,HF}}$. Finally, $\Delta^{1,088}$ was determined to be

$$\Delta^{1,088} = \nu^{1,088,\mathrm{C}}_{\mathrm{m}} - \nu^{1,088,\mathrm{C}}_{\mathrm{g}} = 320(30)\ \mathrm{MHz},$$

in which we used $\nu^{1,088,\mathrm{C}}_{\mathrm{g}}$ reported in refs. 7,8.

We note that the hole-burning effect between the 690-nm and 984-nm transitions, for which the 690-nm radiation burned a hole in the spectrum of the 984-nm transition, may induce a frequency shift in the measurement of $\nu^{690}_{\mathrm{m,HF}}$ for the following reason. The hyperfine transition $|5f^2F_{5/2}, F_{\mathrm{m}} = 1\rangle \rightarrow |6d^2D_{5/2}, F_{\mathrm{m}} = 2\rangle$ (690 nm) used to determine $\nu^{690}_{\mathrm{m,HF}}$ shares the hyperfine state $|6d^2D_{5/2}, F_{\mathrm{m}} = 2\rangle$ with the $|5f^2F_{7/2}, F_{\mathrm{m}} = 3\rangle \rightarrow |6d^2D_{5/2}, F_{\mathrm{m}} = 2\rangle$ transition (984 nm). The frequency difference between the $|5f^2F_{7/2}, F_{\mathrm{m}} = 3\rangle \rightarrow |6d^2D_{5/2}, F_{\mathrm{m}} = 2\rangle$ transition and ν^{984}_{B} was estimated to be only 10 MHz. Therefore, the hole position may overlap with ν^{984}_{B} during the scan of the 690-nm laser frequency in Extended Data Fig. 3a. This changes the fluorescence amplitude of the $^{229\mathrm{m}}Th^{3+}$ signal and may induce frequency shift in the determination of $\nu^{690}_{\mathrm{m,HF}}$. This is because it relies on the amplitude of the $^{229\mathrm{m}}Th^{3+}$ signal (Extended Data Fig. 3b).

To avoid this problem, we used $\nu^{984\prime}_{\mathrm{B}}$ ($= \nu^{984}_{\mathrm{B}} + 540$ MHz) instead of ν^{984}_{B} to determine $\nu^{690}_{\mathrm{m,HF}}$. All of the 984-nm hyperfine transitions using the $|6d^2D_{5/2}, F_{\mathrm{m}} = 2\rangle$ state differ from $\nu^{984\prime}_{\mathrm{B}}$ by more than 500 MHz, which is larger than the Doppler width of the 984-nm spectrum. As a result, a hole related to the $|6d^2D_{5/2}, F_{\mathrm{m}} = 2\rangle$ state did not appear and the signal intensities of the isomer spectra shown in Extended Data Fig. 3a were not affected by the hole-burning effect described above.

Finally, we observed all hyperfine peaks of the 690-nm and 1,088-nm transitions, as shown in Extended Data Fig. 4. The centre frequencies of all the observed peaks agreed with the frequencies estimated from our results within the uncertainties.

Derivation of nuclear properties of $^{229\mathrm{m}}Th$

The magnetic dipole moment of $^{229\mathrm{m}}Th$ (μ_{m}) was derived from $A_{\mathrm{m}}/A_{\mathrm{g}} = (\mu_{\mathrm{m}}/\mu_{\mathrm{g}})(I_{\mathrm{g}}/I_{\mathrm{m}})$. Using A_{m} determined in this study, A_{g} reported in ref. 8 and the μ_{g} ($= 0.366(6)\ \mu_{\mathrm{N}}$) calculated in ref. 28, we determined $\mu_{\mathrm{m}} = -0.378(8)\ \mu_{\mathrm{N}}$ A spectroscopic electric quadrupole moment of $^{229\mathrm{m}}Th$ ($Q^{\mathrm{s}}_{\mathrm{m}}$) was obtained as $Q^{\mathrm{s}}_{\mathrm{m}} = Q^{\mathrm{s}}_{\mathrm{g}}(B_{\mathrm{m}}/B_{\mathrm{g}})$. With the $Q^{\mathrm{s}}_{\mathrm{g}} = 3.11(2)\ e$b calculated in ref. 28 and B_{g} reported in ref. 8, we determined $Q^{\mathrm{s}}_{\mathrm{m}} = 1.77(2)\ e$b. From the relationship between the intrinsic and spectroscopic quadrupole moment[25] $Q^{\mathrm{s}} = Q^0(3K^2 - I(I+1))/((I+1)(2I+3))$, in which $K = I$ in the case of ^{229}Th, we derived the intrinsic electric quadrupole moment of $^{229\mathrm{m}}Th$ to be $Q^0_{\mathrm{m}} = 8.84(10)\ e$b.

The isomer shift $\Delta^{1,088}$ is induced purely by a field shift and can be described by $\Delta^{1,088} = F_{\mathrm{FS}}(\langle r^2_{229\mathrm{m}}\rangle - \langle r^2_{229\mathrm{g}}\rangle)$, in which F_{FS} is the field-shift constant[29]. The mass shift vanishes because $^{229\mathrm{g}}Th^{3+}$ and $^{229\mathrm{m}}Th^{3+}$ have equal masses. Using F_{FS} calculated in ref. 29, we determined $\langle r^2_{229\mathrm{m}}\rangle - \langle r^2_{229\mathrm{g}}\rangle = 0.0097(26)\ \mathrm{fm}^2$. The $\langle r^2_{229\mathrm{m}}\rangle - \langle r^2_{229\mathrm{g}}\rangle$ value can also be estimated from $(\langle r^2_{229\mathrm{m}}\rangle - \langle r^2_{229\mathrm{g}}\rangle)/(\langle r^2_{232}\rangle - \langle r^2_{229\mathrm{g}}\rangle) \approx \Delta^{1,088}/\delta^{1,088}$, in which $(\langle r^2_{232}\rangle - \langle r^2_{229\mathrm{g}}\rangle)$ is the difference in the mean-square radii between ^{232}Th and $^{229\mathrm{g}}Th$. $\delta^{1,088}$ is the isotope shift of the $5f^2F_{5/2} \leftrightarrow 6d^2D_{3/2}$ transition between $^{232}Th^{3+}$ and $^{229\mathrm{g}}Th^{3+}$ ($\delta^{1,088} = \nu^{1,088}_{232} - \nu^{1,088}_{229\mathrm{g}}$). Here we assume that, for heavy ions such as Th, the isotope shift is mainly caused by the field shift, which is proportional to the square of the nuclear charge radius. Using the isotope shift and $\langle r^2_{232}\rangle - \langle r^2_{229\mathrm{g}}\rangle$ reported in refs. 8,48, we estimated $\langle r^2_{229\mathrm{m}}\rangle - \langle r^2_{229\mathrm{g}}\rangle = 0.0097(11)\ \mathrm{fm}^2$, which agrees with the value presented above.

Using the nuclear moment of $^{229\mathrm{g}}Th$ calculated in ref. 28, the change of the Coulomb energy between $^{229\mathrm{g}}Th$ and $^{229\mathrm{m}}Th$ can be described by $\Delta E_{\mathrm{C}} = -485.6\ \mathrm{MeV}(\langle r^2_{229\mathrm{m}}\rangle/\langle r^2_{229\mathrm{g}}\rangle - 1) + 11.69\ \mathrm{MeV}(Q^0_{\mathrm{m}}/Q^0_{\mathrm{g}} - 1)$ (refs. 19,25,29). By using $\langle r^2_{229\mathrm{g}}\rangle = 33.13(16)\ \mathrm{fm}^2$ (ref. 49), we derived $\Delta E_{\mathrm{C}} = 0.04(11)$ MeV. The sensitivity K of the ^{229}Th nuclear clock frequency to the variation of the fine-structure constant can be described by $K = \Delta E_{\mathrm{C}}/E_{\mathrm{isomer}}$ (ref. 29). Using the isomer energy[13] $E_{\mathrm{isomer}} = 8.338(24)$ eV, the sensitivity K was estimated to be $4(13) \times 10^3$.

Exclusion of $^{228}Th^{3+}$ signal

Because the chemical purification of ^{233}U (containing ^{232}U) was carried out approximately 18 months before the measurement, the decay chain from ^{229}Th onwards reached the radiative equilibrium. We estimated that the emission rates of daughter nuclides of ^{229}Th were about 1×10^{-4} relative to the emission rate of ^{229}Th. Among the daughter nuclides, $^{228}Th^{3+}$ generated from ^{232}U has resonances close to the $^{229\mathrm{m}}Th^{3+}$ signals.

Although the presence of $^{228}Th^{3+}$ is estimated to be 5×10^{-4} of $^{229}Th^{3+}$, we calculated the isotope shift between $^{229}Th^{3+}$ and $^{228}Th^{3+}$.

For heavy ions such as Th, the main contribution of the isotope shift is the field shift. Therefore, the isotope shift between $^{229}Th^{3+}$ and $^{228}Th^{3+}$ can be calculated by $\Delta f_{229-228} = F_{FS}\Delta\langle r^2\rangle$. The field-shift constants F_{FS} for all electronic levels relevant to this study are calculated in ref. 29. The difference in mean-square radius between ^{229}Th and ^{228}Th ($\Delta\langle r^2\rangle$) was experimentally determined in ref. 50. As a result, the frequency difference between ^{229m}Th and ^{228}Th was estimated to be −4.1 GHz for the 1,088-nm transition, −4.3 GHz for the 690-nm transition and −4.1 GHz for the 984-nm transition. This indicates that the $^{228}Th^{3+}$ resonance frequencies are at least 1.7 GHz (the 1,088-nm transition), 2.4 GHz (the 690-nm transition) and 2.1 GHz (the 984-nm transition) away from the nearest hyperfine resonance of $^{229m}Th^{3+}$.

Furthermore, high-resolution spectra can be observed only when three laser frequencies are simultaneously resonant to the specific transitions, with an accuracy of approximately 200 MHz for the 1,088-nm and 690-nm transitions and a few GHz for the 984-nm transition. Therefore, the possibility that the observed signals originated from other Th isotopes or atomic species was excluded.

Data availability

The data that support the findings of this study are available from the corresponding author on request.

46. Bollen, G. "Ion surfing" with radiofrequency carpets. *Int. J. Mass Spectrom.* **299**, 131–138 (2011).
47. Kopfermann, H. Nuclear moments. *Nucl. Phys.* **16**, 188 (1960).
48. Safronova, M. S. et al. Nuclear charge radii of ^{229}Th from isotope and isomer shifts. *Phys. Rev. Lett.* **121**, 213001 (2018).
49. Angeli, I. & Marinova, K. P. Table of experimental nuclear ground state charge radii: an update. *At. Data Nucl. Data Tables* **99**, 69–95 (2013).
50. Kälber, W. et al. Nuclear radii of thorium isotopes from laser spectroscopy of stored ions. *Z. Phys. A* **334**, 103–108 (1989).

Acknowledgements The ^{233}U sample used in this paper was provided by the ^{233}U cooperation project between the Japan Atomic Energy Agency and the Inter-University Cooperative Research Program of the Institute for Materials Research, Tohoku University (proposal nos. 17K0204, 17F0011 and 18F0014). This work was supported by JST PRESTO (grant number JPMJPR1868), JSPS KAKENHI (grant nos. JP19H00685, JP21H04473, JP22H04946 and JP23H00094) and Yamada Science Foundation.

Author contributions A.Y. and Y.S. contributed to building the experimental setup, performed the measurements and analysed the data. A.Y., Y.S., H.Ki., K.S. and H.H. contributed to developing the ^{233}U source. M.W. contributed to developing the ion manipulation system, including an RF carpet and a PCB-based quadrupole ion guide. All works were supervised by H.Ka., H.H. and M.W. All authors discussed the results and contributed to the manuscript.

Competing interests The authors declare no competing interests.

Additional information
Correspondence and requests for materials should be addressed to Atsushi Yamaguchi.
Peer review information *Nature* thanks Xu Wang and the other, anonymous, reviewer(s) for their contribution to the peer review of this work.

Reprints and permissions information is available at http://www.nature.com/reprints.

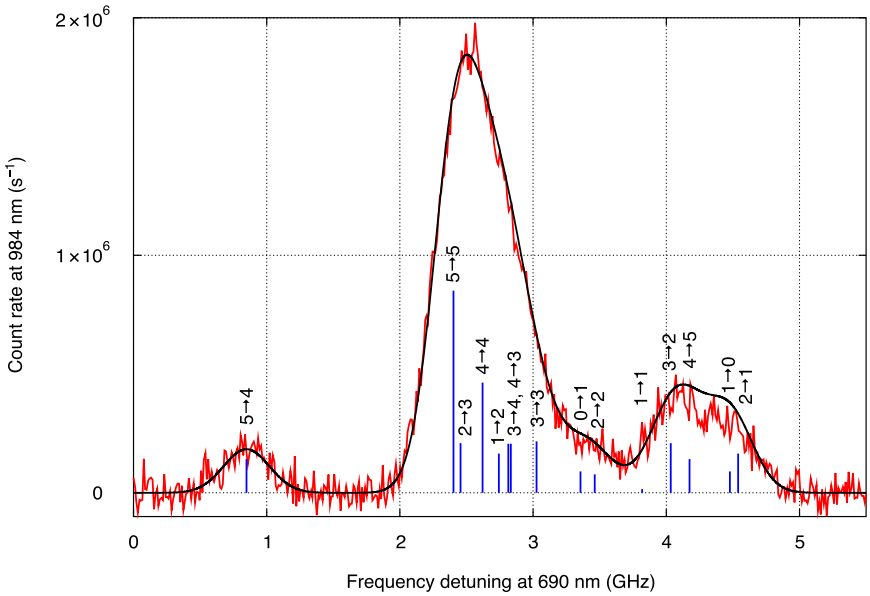

Extended Data Fig. 1 | Doppler-broadened spectrum of the $5f\ ^2F_{5/2} \leftrightarrow 6d\ ^2D_{5/2}$ transition of $^{229g}Th^{3+}$. The red curve represents the background-subtracted fluorescence count rate at 984 nm as a function of the 690-nm laser frequency. Vertical blue bars denote hyperfine transitions ($F_g^i \rightarrow F_g^f$) whose frequencies were calculated on the basis of refs. 7,8. The relative height of the blue bars represents the relative strength of the calculated absorption cross-sections of each hyperfine transition. The black curve represents the summation of Gaussian functions corresponding to each hyperfine transition, for which the width and scaling factor were determined from the fitting of the isolated $5 \rightarrow 4$ peak.

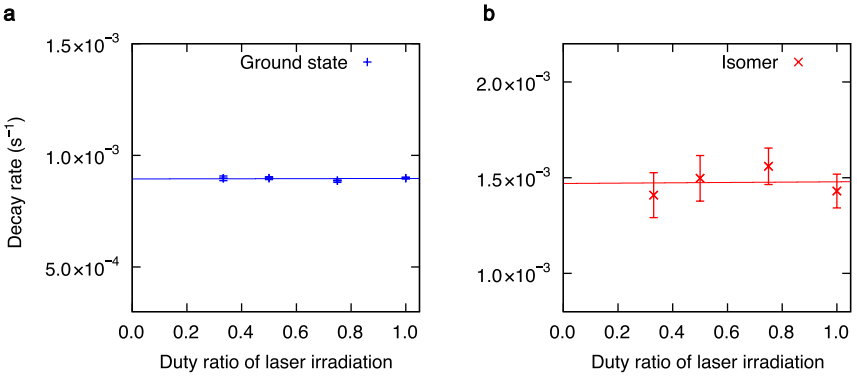

Extended Data Fig. 2 | Dependence of decay rate on laser irradiation time. Dependence of the decay rate on the duty ratio of the laser irradiation time was evaluated for $^{229g}Th^{3+}$ (**a**) and $^{229m}Th^{3+}$ (**b**). Each decay-rate measurement was conducted by repeating a 24-s sequence, in which all three lasers were on for t_{ON} s and off for $(24 - t_{ON})$ s. The duty ratio is calculated as $t_{ON}/24$. The error bars represent the standard deviation of the mean. From the linear fitting shown as a solid line, the decay rate for no laser irradiation was estimated to be $8.94(11) \times 10^{-4}$ s^{-1} for the ground state and $1.47(15) \times 10^{-3}$ s^{-1} for isomer.

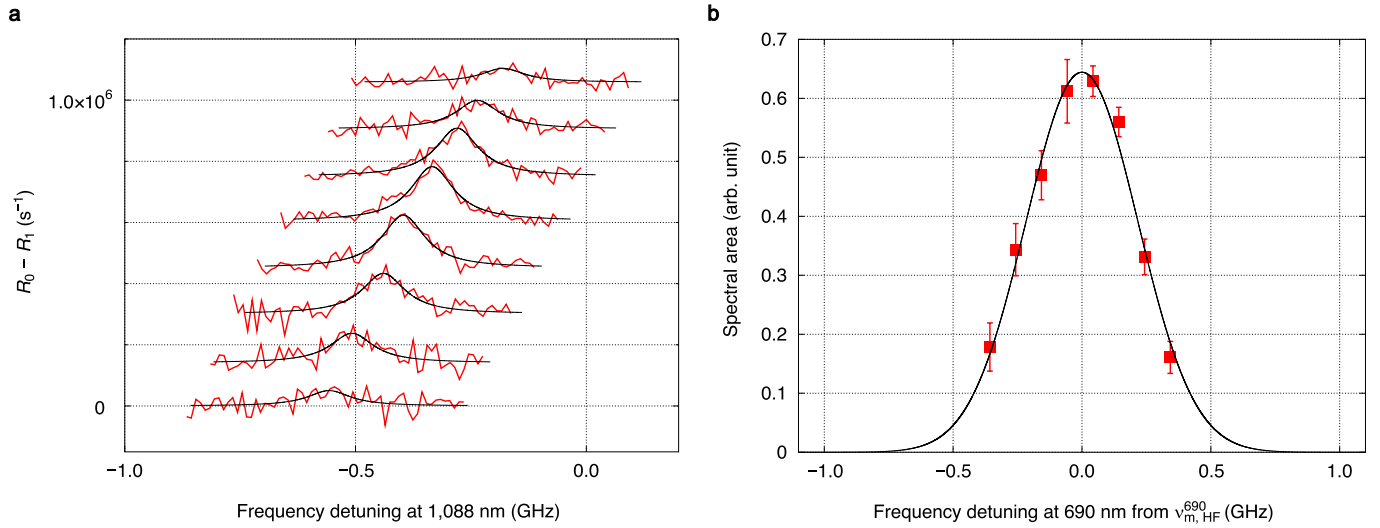

Extended Data Fig. 3 | Determination of the resonance frequency ($\nu^{690}_{m,HF}$) of the $|5f\,^2F_{5/2}, F_m = 1\rangle \rightarrow |6d\,^2D_{5/2}, F_m = 2\rangle$ transition. a, The spectra of the $|5f^2F_{5/2}, F_m = 1\rangle \rightarrow |6d^2D_{3/2}, F_m = 2\rangle$ transition (1,088 nm) were measured with several 690-nm laser frequencies around the resonance frequency of the $|5f^2F_{5/2}, F_m = 1\rangle \rightarrow |6d^2D_{5/2}, F_m = 2\rangle$ transition. From bottom to top, the 690-nm laser frequency was increased by 100 MHz at each step. The spectra were vertically shifted by 1.5×10^5 s^{-1} at each step for clarity. **b**, The spectral area was determined by fitting (black line) and plotted as a function of the 690-nm laser frequency. The resonance frequency $\nu^{690}_{m,HF}$ was determined to be the one that gives the largest spectral area. The error bars represent the standard deviation of the mean.

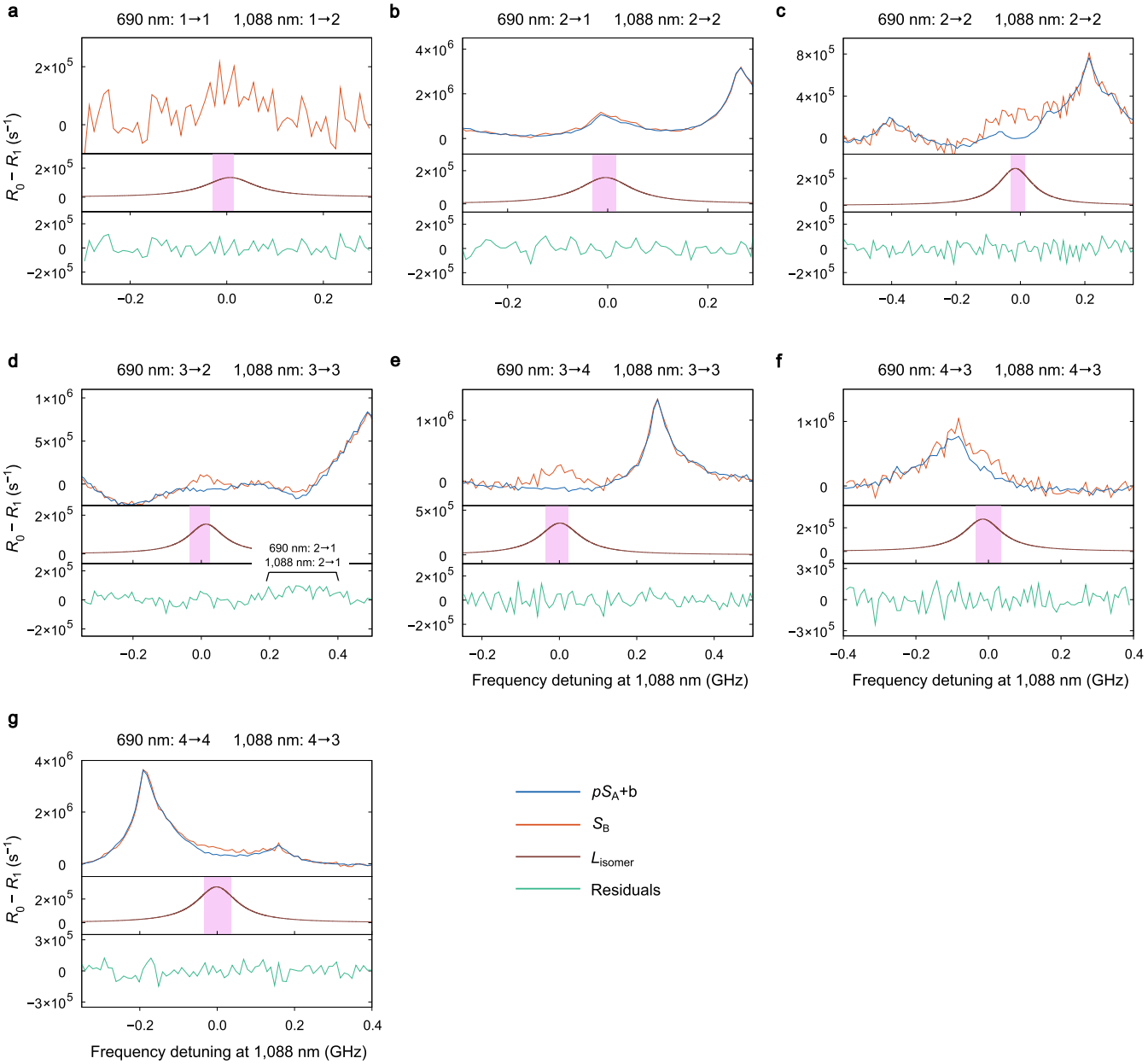

Extended Data Fig. 4 | Observations of all $^{229m}Th^{3+}$ hyperfine resonances on the $5f\ ^2F_{5/2} \rightarrow 6d\ ^2D_{3/2}$ and $5f\ ^2F_{5/2} \rightarrow 6d\ ^2D_{5/2}$ transitions. a–g, All of the hyperfine transitions on the $5f^2F_{5/2} \rightarrow 6d^2D_{3/2}$ (1,088 nm) and $5f^2F_{5/2} \rightarrow 6d^2D_{5/2}$ (690 nm) transitions, which were not contained in Fig. 3b–d, were observed. Definitions of the blue, orange, brown and green curves are same as in Fig. 3b–d. The purple bars indicate the resonance frequencies of each transition calculated using the hyperfine constants and isomer shifts obtained in this study. The width of the purple bar represents the uncertainty of the calculated values. The corresponding hyperfine transitions $|5f\ ^2F_{5/2}, F_m^{i,690}\rangle \rightarrow |6d\ ^2D_{5/2}, F_m^{f,690}\rangle$ (690 nm) and $|5f\ ^2F_{5/2}, F_m^{i,1,088}\rangle \rightarrow |6d\ ^2D_{3/2}, F_m^{f,1,088}\rangle$ (1,088 nm) are shown at the top of each figure as $F_m^{i,690} \rightarrow F_m^{f,690}$ and $F_m^{i,1,088} \rightarrow F_m^{f,1,088}$. We measured the spectrum **a** only with ν_B^{984} because there were no overlapped $^{229g}Th^{3+}$ resonances in the scanned frequency range.